The International Journal of Robotics Research
http://ijr.sagepub.com

Hybrid Adaptive Vision Force Control for Robot Manipulators Interacting with Unknown Surfaces

Antonio C. Leite, Fernando Lizarralde and Liu Hsu
The International Journal of Robotics Research 2009; 28; 911
DOI: 10.1177/0278364909101932

Antonio C. Leite
Fernando Lizarralde
Liu Hsu
Department of Electrical Engineering
COPPE,
Federal University of Rio de Janeiro,
Rio de Janeiro,
RJ 21945-970, Brazil
{toni, fernando, liu}@coep.ufrj.br

Hybrid Adaptive Vision–Force Control for Robot Manipulators Interacting with Unknown Surfaces

Abstract

A hybrid control scheme based on adaptive visual servoing and direct force control is proposed for robot manipulators to perform interaction tasks on smooth surfaces. The camera parameters, as well as the constraint surface, are considered to be uncertain. A fixed camera with optical axis non-perpendicular to the robot workspace is used for position control, while a force sensor mounted on the robot wrist is used for force regulation. In order to solve the interaction problem on unknown surfaces, a method is developed to estimate the constraint geometry and keep the end-effector orthogonal to the surface at the contact point, during the task execution. Experimental results are presented to illustrate the performance and feasibility of the proposed scheme.

KEY WORDS—adaptive control, force control, robot vision, robotic manipulators.

1. Introduction

In advanced robotic applications, autonomy and flexibility are fundamental requirements for robots to operate in unstructured environments, where the physical or geometrical description of the workspace is partially known. In this context, one way to increase these abilities in practical tasks (e.g. deburring, polishing, welding, etc.) is to integrate a number of different sensors into the robot system.

Cameras are useful robotic sensors since they mimic the human sense of vision and allow the robots to locate and inspect the environment without contact. On the other hand, force sensors are useful to control the contact force or to monitor the interaction forces in order to avoid damages in the robot end-effector and manipulated objects. Thus, an interesting solution is to combine visual servoing and force control in a *hybrid control* scheme so that the advantages of each sensing mode may be simultaneously achieved for a given interaction task.

1.1. Previous Works

The benefits of combining vision and force sensing within the feedback loop of a robot manipulator were presented by Nelson et al. (1995) through three different approaches: in *traded control*, a task space direction is alternately controlled using a vision sensor or force sensor; in *hybrid control*, different directions of the task space are simultaneously controlled using vision and force sensors; in *shared control*, both vision and force sensors control the same direction of the task space simultaneously. In this framework, several hybrid controllers were proposed to use the information obtained from vision and force sensors in order to control the robot configuration (position and orientation) during the task execution (Pichler and Jägersand 2000; Baeten and De Schutter 2002; Carelli et al. 2004; Lippielo et al. 2006). However, only a few control strategies deal with the parametric uncertainties in the camera, robot and constraint surface.

Hosoda et al. (1998) proposed a hybrid control scheme that uses on-line estimators for the constraint geometry and the camera–robot system parameters. For this purpose, the designed controller only requires prior knowledge of the kinematics mapping. Following this same research line, Xiao et al. (2000) developed a control strategy based on a computed torque method to combine force and vision sensing, in order

The International Journal of Robotics Research
Vol. 28, No. 7, July 2009, pp. 911–926
DOI: 10.1177/0278364909101932

Figures 1–3, 5–10 appear in color online: http://ijr.sagepub.com to solve the three-dimensional tracking problem on unknown surfaces. In this approach, the robot dynamics was assumed to be fully known and a recursive least-squares algorithm was used to cope with the camera misalignment. A hybrid control method using vision and force sensors to perform tasks on unknown planar surfaces was presented by Olsson et al. (2002) and Chang (2004). However, in these strategies the camera needs to be calibrated with respect to the robot base frame.

A hybrid vision–force controller for robot manipulators with uncertain kinematics, dynamics and constraint surface was proposed by Zhao and Cheah (2004). The control algorithm is based on an adaptive law with force and gravity regressors. Nevertheless, the uncertainties in the camera model were not rigorously taken into account in the theoretical analysis. A scheme for adaptive visual servoing of the constrained planar robots with uncertainties was proposed by Dean-León et al. (2006). The control algorithm is based on the second-order sliding mode approach and a visual compensator for the joint dynamic and viscous contact friction is presented. However, an explicit solution to solve the interaction problem on unknown surfaces was not considered.

On the other hand, some approaches have been proposed for on-line estimation of the constraint geometry in the absence of vision sensing (Namvar and Aghili 2004; Karayiannidis and Doulgeri 2006) or integrating both instantaneous task specification and estimation of geometric uncertainty in a unified framework (De Schutter et al. 2007) in order to perform more complex tasks.

1.2. Contribution

In this paper, the vision and force control problem for non-redundant robot manipulators using a fixed uncalibrated camera and a force sensor (Figure 1) is considered. A hybrid control method is proposed to combine adaptive visual servoing and direct force control in the presence of uncertainties in the camera parameters (intrinsic and extrinsic) and smooth surfaces with unknown geometry.

The visual servoing strategy is based on a symmetrization method via factorization of the control matrix to solve the multivariable adaptive control problem (Costa et al. 2003). The adaptive algorithm is robust in the sense that it presents reduced sensitivity to kinematic uncertainties. The force control strategy is based on an integral action, owing to its well-known robustness with respect to the measurement time delay and capability of removing the force disturbances (Wilfinger et al. 1994).

In order to solve the interaction problem on unknown surfaces, a method is presented to estimate the constraint geometry and reorientate the end-effector on the surface during the task execution using force and displacement on-line measurements (Yoshikawa and Sudou 1993). The orientation control uses the unit quaternion formulation which is free of singularities and computationally efficient (Sciavicco and Siciliano 2000). Based on a cascade control strategy (Guenther and Hsu 1993), an extension of the proposed control method to consider the robot dynamics is also discussed. Experimental results are presented to illustrate the practical performance and viability of the proposed scheme.

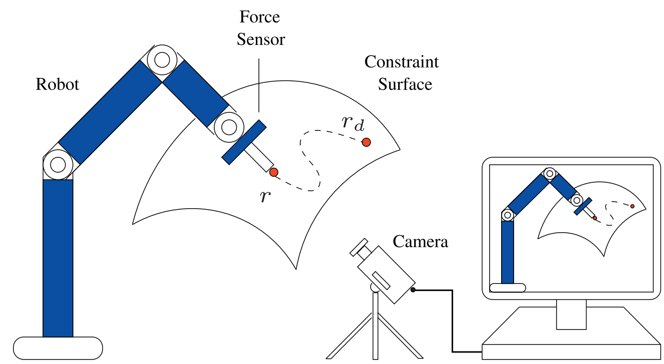

Fig. 1. Vision–force robot system.

2. Kinematic Control

In this section, the kinematic control problem for a robot manipulator is considered. Let $x = [x_1 \quad x_2 \quad x_3]^{\mathrm{T}}$ be the end-effector position with respect to the robot base, expressed in the tool frame $\bar{E}_e$. In addition, let R_{be} be the rotation matrix of the tool frame $\bar{E}_e$ with respect to the base frame $\bar{E}_b$ and $q = [q_s \quad q_v^{\mathrm{T}}]^{\mathrm{T}}$ be the unit quaternion representation for R_{be}, where $q_s \in \mathbb{R}$ and $q_v \in \mathbb{R}^3$ are the scalar and vectorial part of the quaternion respectively, constrained by the condition $\|q\| = 1$ (Sciavicco and Siciliano 2000). In this context, the end-effector configuration $r = [x \quad q]^{\mathrm{T}} \in \mathbb{R}^m$ is given by the forward kinematics map $r = k(\theta)$, where $\theta \in \mathbb{R}^n$ is the vector of manipulator joint angles. Note that, considering a robot arm with six degrees of freedom (DOFs), $m = 7$ and $n = 6$.

The differential kinematics equation can be obtained as the time-derivative of the forward kinematics given by

$$\dot{r} = \begin{bmatrix} \dot{x} \\ \dot{q} \end{bmatrix} = J_k(\theta)\dot{\theta}, \tag{1}$$

where

$$J_k(\theta) = \frac{\partial k(\theta)}{\partial \theta} \in \mathbb{R}^{m \times n}$$

is the analytical Jacobian. The end-effector velocity $v = [\dot{x} \quad \omega]^{\mathrm{T}}$, composed by the linear velocity $\dot{x}$ and the angular velocity ω, both expressed in the tool frame $\bar{E}_e$, is related to $\dot{r}$ by

$$v = \begin{bmatrix} \dot{x} \\ \omega \end{bmatrix} = \begin{bmatrix} I & 0 \\ 0 & 2J_q(q) \end{bmatrix} \begin{bmatrix} \dot{x} \\ \dot{q} \end{bmatrix} = J_r(q)\dot{r}, \tag{2}$$

where $J_q(q) = [-q_v \quad q_s I + (q_v \times)]$ and $J_r(q)$ is the representation Jacobian. Then, substituting (1) into (2) gives

$$\upsilon = J_r(q) J_k(\theta)\dot{\theta} = J(\theta)\dot{\theta}, \tag{3}$$

where $J(\theta) \in \mathbb{R}^{n\times n}$ is the manipulator Jacobian. Thus, from (3) and considering $\dot{\theta}_i$ as the control input u_i ($i = 1, \ldots, n$) one obtains the following control system:

$$\upsilon = J(\theta)u. \tag{4}$$

A cartesian control law υ_c can be transformed to joint control signals by using

$$u = J(\theta)^{-1}\upsilon_c = J(\theta)^{-1}\begin{bmatrix}\upsilon_x\\ \upsilon_q\end{bmatrix}, \tag{5}$$

provided that $\upsilon_c(t)$ does not drive the robot to *singular configurations*. Therefore, from (4) and (5) one has that

$$\begin{bmatrix}\dot{x}\\ \omega\end{bmatrix} = \begin{bmatrix}\upsilon_x\\ \upsilon_q\end{bmatrix}, \tag{6}$$

and, naturally, υ_x and υ_q are designed to control the end-effector position and orientation, respectively. Here, the following two assumptions are considered:

(A1) the robot kinematics is *known*;

(A2) the robot dynamics is *negligible*.

The last assumption is applicable to most commercial robots with high gear ratios and/or when the task speed is slow.

3. Hybrid Control Scheme

The hybrid control method combines force and torque information with end-effector position and orientation data, according to the concept of complementary orthogonal subspaces in force and motion formalized by Mason (1981). In this framework, the efficiency of the hybrid control method was first experimentally verified on a Scheinman–Stanford arm (Raibert and Craig 1981).

Some issues regarding *dependence on the choice of units* and *dimensional inconsistency* of the orthogonal complements concept in the hybrid control theory were raised by Duffy (1990). However, the hybrid control scheme proposed in this section is free from such problems, since: (a) the control actions can be split and treated separately in translational and rotational motions; and (b) the formulation of the control scheme only requires the end-effector position and the interaction force between the end-effector and environment, respectively.

Hence, the position and force constraints can be separately considered and the controllers are not affected by mutual interferences. These constraints are specified in an appropriate coordinate system for the task execution named the *constraint frame* and denoted by $\bar{E}_s$. From the selection matrices $S \in \mathbb{R}^{3\times 3}$ and $I - S$, that determine which DOFs must be controlled by force and position, the control signals are decoupled and the control laws for each subspace can be independently designed in order to achieve simultaneously different force and position requirements for a given task. Thus, the hybrid control law is given by

$$\upsilon_x = \upsilon_{hp} + \upsilon_{hf}, \tag{7}$$

where υ_{hp} and υ_{hf} are the decoupled control signals acting, respectively, in the position and force subspaces, such that

$$\upsilon_{hp} = R_{es}(I - S)R_{es}^{\mathrm{T}}\upsilon_p, \quad \upsilon_{hf} = R_{es} S R_{es}^{\mathrm{T}}\upsilon_f, \tag{8}$$

where υ_p is the position control signal, υ_f is the force control signal and R_{es} is the rotation matrix of the constraint frame $\bar{E}_s$ with respect to the tool frame $\bar{E}_e$.

Now, considering that the constraint surface in the task space can be described by $\varphi(x) = 0$, where $\varphi(x) : \mathbb{R}^n \mapsto \mathbb{R}$ is a smooth mapping, the constrained motion of the end-effector on the surface satisfies

$$D(x)\dot{x} = 0,$$

where

$$D(x) = \frac{\partial\varphi(x)}{\partial x}$$

denotes the *normal vector* of the constraint surface. Then, when the constraint geometry is *known* the constraint frame $\bar{E}_s = [\mathbf{x}_s \quad \mathbf{y}_s \quad \mathbf{z}_s]$ can be conveniently chosen with unit normal vector

$$\mathbf{z}_s(x) = \frac{D(x)}{||D(x)||}$$

and *arbitrary* orthonormal vectors $\mathbf{x}_s$, $\mathbf{y}_s$. Thus, the rotation matrix of the constraint frame $\bar{E}_s$ with respect to the base frame $\bar{E}_b$ can be derived by

$$R_{bs} = [(\mathbf{x}_s)_b \quad (\mathbf{y}_s)_b \quad (\mathbf{z}_s)_b],$$

and the desired orientation of the end-effector on the constraint surface can be obtained by

$$R_d = R_{bs}(R_{es})_d^{\mathrm{T}}, \tag{9}$$

where $(R_{es})_d$ denotes the desired rotation matrix of the constraint frame $\bar{E}_s$ with respect to the tool frame $\bar{E}_e$.

Remark 1. Without loss of generality, the reorientation of the end-effector on the constraint surface considers the alignment problem of the tool frame $\bar{E}_e$ with respect to the constraint frame $\bar{E}_s$, such that $(R_{es})_d = I$ and thus $R_d = R_{bs}$.

Remark 2. For a *non-planar* surface, the orientation of the constraint frame $\bar{E}_s$ with respect to the base frame $\bar{E}_b$ depends on the end-effector position x on the constraint surface, that is, $R_{bs} = R_{bs}(x)$.

3.1. Position Control

Consider the position control problem for a kinematic manipulator. Here, one assumes that the control goal is to track the desired *time-varying* trajectory $x_d(t)$ from the current position x, that is,

$$x \to x_d(t), \quad e_p = x_d - x \to 0, \tag{10}$$

where e_p is the position error. Considering $\upsilon_x = \upsilon_p$ and from (6), one has that $\dot{x} = \upsilon_p$. Thus, using a feedforward plus proportional control law

$$\upsilon_p = \dot{x}_d + K_x e_p, \tag{11}$$

where $K_x = k_x I$ and the position error dynamics is governed by $\dot{e}_p + K_x e_p = 0$. Hence, by a proper choice of k_x as a positive constant, $e_p \to 0$ exponentially as $t \to \infty$.

3.2. Force Control

Consider the force control problem for a kinematic manipulator. Here, one assumes that the control goal is to regulate the measured contact force f to a *constant* desired force f_d along the constraint surface, that is,

$$f \to f_d, \quad e_f = f - f_d \to 0, \tag{12}$$

where e_f is the force error. Similar to *Hooke's law*, the contact force can be modeled by

$$f = -K_s(x - x_s), \tag{13}$$

where x is the position of the contact point, x_s is a point of the surface at rest, $K_s = k_s I$ is the stiffness matrix and $k_s > 0$ is the stiffness coefficient.

In general, force measurements may be corrupted by noise and thus a first-order filter is used to reduce this effect

$$\tau_f \dot{\hat{e}}_f = -\hat{e}_f + e_f, \tag{14}$$

where $\hat{e}_f$ is the filtered force error and $\tau_f > 0$ is the filter time constant. Then, from (12), (13) and (14) the force error equation is given by $\tau_f \ddot{\hat{e}}_f + \dot{\hat{e}}_f = -K_s \dot{x}$. Considering $\upsilon_x = \upsilon_f$, then from (6), one has that $\dot{x} = \upsilon_f$. Thus, using a proportional plus integral control law

$$\upsilon_f = K_p \hat{e}_f + K_i \int_0^t \hat{e}_f(\tau) d\tau, \tag{15}$$

where $K_p = k_p I$ and $K_i = k_i I$, the force error dynamics is governed by $\tau_f \dddot{\hat{e}}_f + \ddot{\hat{e}}_f + k_s k_p \dot{\hat{e}}_f + k_s k_i \hat{e}_f = 0$. Hence, for a proper choice of k_p and k_i as positive constants satisfying $k_p > k_i \tau_f$, the closed-loop system is exponentially stable and, consequently, $\dot{\hat{e}}_f, \hat{e}_f \to 0$ and $e_f \to 0$ as $t \to \infty$. Note that a pure proportional control action is not enough to attenuate input disturbances and guarantee an acceptable performance simultaneously.

3.3. Orientation Control

Consider the orientation control problem for a kinematic manipulator. Here, one assumes that the control goal is to drive the current orientation matrix $R \in SO(3)$ to a desired *time-varying* attitude $R_d(t)$, that is,

$$R \to R_d(t), \quad R_q = R^{\mathrm{T}} R_d \to I, \tag{16}$$

where $R_q \in SO(3)$ is the orientation error matrix expressed in the tool frame $\bar{E}_e$. Note that, taking $R = R_{be}$ and from (9), one has that $R_q = R_{es}(R_{es})_d^{\mathrm{T}}$.

Let $e_q = [e_{qs} \quad e_{q\upsilon}^{\mathrm{T}}]^{\mathrm{T}}$ be the unit quaternion representation for R_q such that $e_q = q^{-1} * q_d(t)$, where q_d is the unit quaternion representation for R_d and "$*$" denotes the quaternion product operator. Note that, $e_q = [1 \quad 0^{\mathrm{T}}]^{\mathrm{T}}$ if and only if R and R_d are aligned. Thus, from (6) one has that $\omega = \upsilon_q$ and using a feedforward plus proportional control law

$$\upsilon_q = \omega_d + K_o e_{q\upsilon}, \tag{17}$$

where ω_d is the desired angular velocity and K_o is a positive definite matrix, the equilibrium point $(e_{qs}, e_{q\upsilon}) = (\pm 1, 0)$ is *almost* globally[1] asymptotically stable (for a proof see Appendix A.1).

Now, let $\xi_p \in \mathbb{R}^2$ be the decoupled position error and $\xi_f \in \mathbb{R}^3$ be the error state vector of the decoupled closed-loop force control system $\dot{\xi}_f = A\xi_f$ ($A \in \mathbb{R}^{3\times 3}$ is Hurwitz), both expressed in the constraint frame $\bar{E}_s$ after selecting the position and force control directions. Noting that $R_d = R_{bs}(x)$, one assumes that the constraint surface is smooth enough and the task speed is not so fast. Thus, the variation of the rotation matrix R_{bs} with respect to x can be neglected, such that

$$\frac{\partial R_{bs}}{\partial x} \otimes \dot{x} \cong 0,$$

where "$\otimes$" denotes the Kronecker product. Then, the following theorem can be stated.

1. In this work, we use the term *almost* globally to indicate that the domain of attraction is the entire state space, except for a set of measure zero.

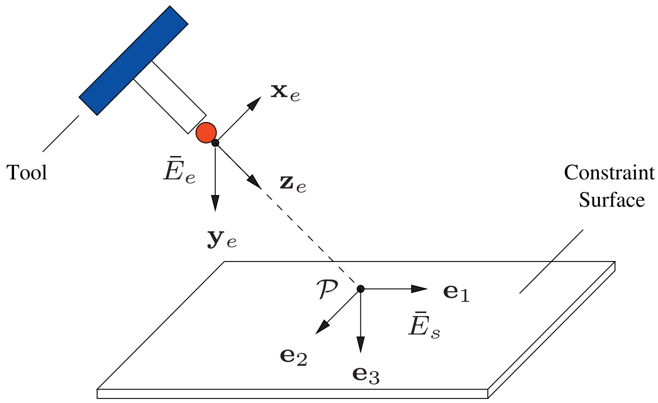

Fig. 2. Constraint frame $\bar{E}_s$ in a contact point on the surface.

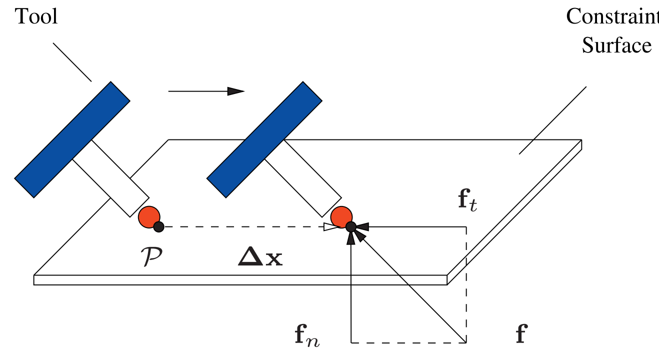

Fig. 3. Tangential and normal forces in a contact point on the surface.

Theorem 1. *Consider the closed-loop system described by (4) and (5), with the hybrid control law given by (7) and (8), and the position controller (11), the force controller (15) and the orientation controller (17). Assume that the reference signal $x_d(t)$ is piecewise continuous and uniformly bounded in norm, f_d is constant and $q_d(t)$ is the unit quaternion representation for $R_d(t) \in SO(3)$. Under the assumptions (A1) and (A2), the following properties hold: (i) all signals of the closed-loop system are uniformly bounded; (ii) $\lim_{t\to\infty} \xi_p(t) = 0$, $\lim_{t\to\infty} \xi_f(t) = 0$ and $\lim_{t\to\infty} e_{qv}(t) = 0$, $\lim_{t\to\infty} e_{qs}(t) = \pm 1$. Thus, the closed-loop system is* almost *globally asymptotically stable.*

Proof. See Appendix A.2. □

4. Unknown Constraint Surface

Considering that the robot manipulator interacts with a partially known environment, it is appropriate to present a method to estimate the *geometric parameters* of the constraint surface (Murray et al. 1994) and update the end-effector orientation during the task execution. Here, one assumes that the constraint surface $\varphi(x) = 0$ is *unknown*. This assumption states that the end-effector position is constrained on an unknown surface with smooth curvature.

In the hybrid control approach it is necessary to separate the motion control and interaction control actions along complementary directions of the task space. However, to achieve this in an unstructured workspace, one has to determine the geometry of the constraint surface and its relationship with the frames of interest. Thus, the decoupling of control variables can be performed in the constraint space, where the task is naturally described and the selection matrices have a diagonal form with 0 and 1 elements.

Then, in a contact point $\mathcal{P}$ on the constraint surface one considers a fixed orthonormal frame $\bar{E}_s = [\mathbf{e}_1 \quad \mathbf{e}_2 \quad \mathbf{e}_3]$, where the vectors $\mathbf{e}_1, \mathbf{e}_2$ belong to a tangent plane to the surface[2] and the vector $\mathbf{e}_3$ is orthogonal to the surface (Figure 2). For a *frictionless* contact point, forces can only be applied in the normal direction to the surface. Thus, based on the contact force $\mathbf{f}$ which is exerted by the end-effector on the surface, one defines

$$\mathbf{e}_3 = -\mathbf{f}/\|\mathbf{f}\|$$

as the estimated normal vector of the constraint surface. However, considering a contact point with *friction*, forces can be exerted in any direction within the *friction cone* (Murray et al. 1994). Therefore, contact loss or sliding on the surface are precluded.

Moreover, when a *frictional* surface is considered, the contact force $\mathbf{f}$ has a tangential component (Figure 3). Here, one assumes that the only action of tangential forces is due to the *friction force* and it acts in the opposed direction of the end-effector displacements. Then, the estimated normal vector of the constraint surface can be rewritten as

$$\mathbf{e}_3 = -(\mathbf{f} - \mathbf{f}_t)/\|\mathbf{f} - \mathbf{f}_t\|, \tag{18}$$

where the tangential force $\mathbf{f}_t$, aligned with the movement direction, is given by $\mathbf{f}_t = (\mathbf{f} \cdot \mathbf{t})\mathbf{t}$, where $\mathbf{t} = \mathbf{\Delta x}/\|\mathbf{\Delta x}\|$ and $\mathbf{\Delta x}$ is the *infinitesimal* displacement of the end-effector on the constraint surface during the interaction.

Note that any orthonormal vectors $\mathbf{e}_1, \mathbf{e}_2$ in the tangent plane could be chosen to compose $\bar{E}_s$. However, in order to minimize the angle between vectors $\mathbf{x}_e$ and $\mathbf{e}_1$, the projection of vector $\mathbf{x}_e$ on the tangent plane is used to obtain a tangent vector $\mathbf{t}_1$, that is,

$$\mathbf{t}_1 = (I - \mathbf{e}_3\mathbf{e}_3\cdot)\mathbf{x}_e.$$

2. Here, without loss of generality, a planar surface is considered, which is locally a good approximation to surfaces of regular curvature (Sciavicco and Siciliano 2000).

Thus, the estimated tangent vector $\mathbf{e}_1$ can be defined by

$$\mathbf{e}_1 = \mathbf{t}_1/\|\mathbf{t}_1\|, \tag{19}$$

and the vector $\mathbf{e}_2$ can be obtained from right-hand rule, that is, $\mathbf{e}_2 = \mathbf{e}_3 \times \mathbf{e}_1$. Hence, the estimated orientation of the constraint frame $\bar{E}_s$ with respect to the tool frame $\bar{E}_e$ is given by

$$\hat{R}_{es} = [(\mathbf{e}_1)_e \quad (\mathbf{e}_2)_e \quad (\mathbf{e}_3)_e], \tag{20}$$

and, thus, the desired end-effector orientation on the constraint surface can be obtained as $R_d = R_{be}\hat{R}_{es}$.

Remark 3. During the task execution, the estimated tangent vector $\mathbf{e}_1$ can be defined by using the *infinitesimal* displacement $\mathbf{\Delta x}$ of the end-effector on the constraint surface, such that $\mathbf{e}_1 = \mathbf{\Delta x}/\|\mathbf{\Delta x}\|$. However, from the practical point of view, this estimation is more sensitive to sensor measurement noise.

Remark 4. For a *frictionless* contact point, the estimated normal vector $\mathbf{e}_3$ can be defined in terms of the contact force $\mathbf{f}$ only. Thus, an infinitesimal displacement $\mathbf{\Delta x}$ of the end-effector on the constraint surface is not required in order to estimate $\mathbf{e}_1$ and, consequently, $\hat{R}_{es}$. Hence, for a *frictionless* contact point the orientation matrix $\hat{R}_{es}$ can be defined in terms of force measurements only.

5. Visual Servoing

In this work, the visual servoing approach is used to provide closed-loop position control for the robot end-effector. Let $y = [y_1 \quad y_2]^{\mathrm{T}}$ be the position of the image feature (or target) fixed on the end-effector tip and $y_d(t)$ be the desired *time-varying* trajectory, both expressed in the image frame $\bar{E}_v$. Then, the control goal can be described by

$$y \to y_d(t), \quad e_v = y_d - y \to 0, \tag{21}$$

where $e_v = [e_{v_1} \quad e_{v_2}]^{\mathrm{T}}$ is the image error. Here, one considers a 6-DOF robot manipulator performing planar motions in the cartesian space. Hence, without loss of generality, the end-effector position with respect to the robot base, expressed in the base frame $\bar{E}_b$, is given by $\bar{x} = [\bar{x}_1 \quad \bar{x}_2]^{\mathrm{T}}$.

Then, assuming that the camera frame $\bar{E}_c$ and the base frame $\bar{E}_b$ are aligned with respect to the z-axis and considering a monocular fixed CCD camera with optical axis *non-perpendicular* to the robot workspace (Figure 4), the cartesian space can be related to the image space by (Hutchinson et al. 1996)

$$y = K(\bar{x})\bar{x} + r_0, \tag{22}$$

with

$$K(\bar{x}) = \frac{f_0}{f_0 + z(\bar{x})}\begin{bmatrix}\alpha_1 & 0\\ 0 & \alpha_2\end{bmatrix}\begin{bmatrix}\cos(\phi) & -\sin(\phi)\\ \sin(\phi) & \cos(\phi)\end{bmatrix},$$

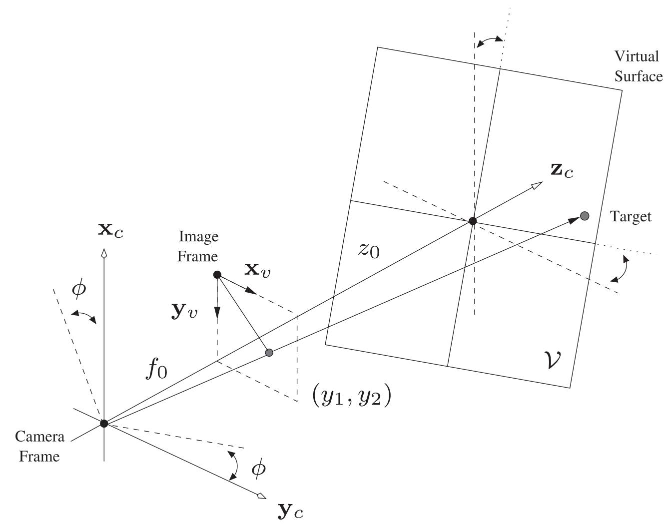

Fig. 4. Virtual surface for image tracking.

where r_0 is a constant term, which depends on the position of the base frame $\bar{E}_b$ with respect to the camera frame $\bar{E}_c$, $K(\bar{x})$ is the *camera/workspace transformation matrix* and considers the camera orientation angle ϕ (or camera misalignment) with respect to the base frame $\bar{E}_b$, f_0 is the focal length of the camera lens, $z(\bar{x})$ is the depth from the image frame $\bar{E}_v$ to the robot workspace (in general, $z(\bar{x}) \gg f_0$), and $\alpha_i > 0$ $(i = 1, 2)$ are the scaling factors of the camera (in pixels per millimeter).

5.1. Virtual Surface

Consider the visual servoing problem for a robot manipulator moving along a desired trajectory specified on a virtual surface $\mathcal{V}$ located in the robot workspace (Figure 4). Then, a generic surface in the cartesian space can be described by the local coordinates $\bar{x}$ as

$$z(\bar{x}) = z_0 + \nu(\bar{x}, c), \tag{23}$$

where z_0 is a constant depth between the image frame $\bar{E}_v$ and robot workspace, $c \in \mathbb{R}^2$ is a vector of constant parameters and $\nu(\cdot)$ is a smooth function. Without loss of generality this work considers the case of *locally flat* surfaces given by

$$z(\bar{x}) = z_0 + \epsilon c^{\mathrm{T}}\bar{x}, \tag{24}$$

where $c = [a \quad b]^{\mathrm{T}}$ and $a, b \in \mathbb{R}$ are constant parameters relative to the surface slope with respect to the axes $\mathbf{x}_c$ and $\mathbf{y}_c$ in the camera frame $\bar{E}_c$, and ϵ is a sufficiently small constant parameter, such that the following condition holds:

$$\epsilon c^{\mathrm{T}}\bar{x} \ll z_0. \tag{25}$$

In order to avoid singularities, one considers that the robot motions in the workspace satisfy the condition (25) and the end-effector always remains visible, avoiding occlusion related problems.

Remark 5. For the general case, where the camera frame $\bar{E}_c$ and the base frame $\bar{E}_b$ are not aligned, the cartesian space can be related to the image space by

$$y = h(x)\alpha R_{\upsilon} x + r_0,$$

where $h(x) = f_0/(f_0 + z(x))$, $\alpha = \text{diag}[\alpha_1, \alpha_2]$ and $R_{\upsilon} \in \mathbb{R}^{2\times 3}$ is the *upper* matrix obtained from $R_{ce} \in \text{SO}(3)$, with R_{ce} being the rotation matrix of the tool frame $\bar{E}_e$ with respect to the camera frame $\bar{E}_c$. However, when the end-effector moves on a two-dimensional virtual surface, one can show that, by an adequate choice of the base frame $\bar{E}_b$, the term x can be replaced by $\bar{x}$ in the above transformation.

5.2. Control Problem

In this work, the cartesian control problem in the image space is described by

$$\dot{y} = G(\bar{x})\upsilon_{\upsilon}, \tag{26}$$

where $\upsilon_{\upsilon} = [\upsilon_{\upsilon_1} \quad \upsilon_{\upsilon_2}]^{\mathrm{T}}$ and $G(\bar{x})$ is an *uncertain matrix* obtained from partial derivative of $K(\bar{x}) = [k_1(\bar{x}) \quad k_2(\bar{x})]$, that is,

$$G(\bar{x}) = K(\bar{x}) + \frac{\partial k_1(\bar{x})}{\partial \bar{x}}\bar{x}_1 + \frac{\partial k_2(\bar{x})}{\partial \bar{x}}\bar{x}_2 \tag{27}$$

and

$$g_{11}(\bar{x}) = \frac{\alpha_1 f_0}{z_c^2}\left[z_c\cos(\phi) + \frac{\partial z(\bar{x})}{\partial \bar{x}_1}h_1(\bar{x})\right],$$

$$g_{12}(\bar{x}) = \frac{\alpha_1 f_0}{z_c^2}\left[-z_c\sin(\phi) + \frac{\partial z(\bar{x})}{\partial \bar{x}_2}h_1(\bar{x})\right],$$

$$g_{21}(\bar{x}) = \frac{\alpha_2 f_0}{z_c^2}\left[z_c\sin(\phi) - \frac{\partial z(\bar{x})}{\partial \bar{x}_1}h_2(\bar{x})\right],$$

$$g_{22}(\bar{x}) = \frac{\alpha_2 f_0}{z_c^2}\left[z_c\cos(\phi) - \frac{\partial z(\bar{x})}{\partial \bar{x}_2}h_2(\bar{x})\right],$$

with $z_c = f_0 + z(\bar{x})$, $h_1(\bar{x}) = \bar{x}_1\cos(\phi) + \bar{x}_2\sin(\phi)$ and $h_2(\bar{x}) = \bar{x}_1\sin(\phi) + \bar{x}_2\cos(\phi)$.

Remark 6. From (26) and using a feedforward plus proportional control law given by

$$\upsilon_{\upsilon} = G(\bar{x})^{-1}[\dot{y}_d + K_{\upsilon}(y_d - y)], \tag{28}$$

the image error dynamics is governed by $\dot{e}_{\upsilon} + K_{\upsilon}e_{\upsilon} = 0$. Hence, by a proper choice of K_{υ} as a positive-definite matrix, $e_{\upsilon} \to 0$ exponentially as $t \to \infty$. However, considering that the intrinsic and extrinsic parameters of the camera model are *uncertain*, the camera/workspace transformation matrix K (and G) is also *uncertain*. Therefore, the control law (28) does not guarantee asymptotic tracking of the desired trajectory, since the closed-loop system cannot be linearized.

Remark 7. In order to simplify the notation, the term $\bar{x}$ will be removed from $G(\bar{x})$. Thus, $G(\bar{x}) = G = [g_{ij}]$ for $i, j = 1, 2$ and $G(\bar{x})^{-1} = G^{-1}$.

5.3. Adaptive Visual Servoing

In the model-reference adaptive control approach (Khalil 2002), the reference model can be specified by

$$\dot{y}_d = -\Lambda y_d + \Lambda y_r, \tag{29}$$

where $y_r \in \mathbb{R}^2$ is the reference signal expressed in the image frame $\bar{E}_{\upsilon}$ and assumed to be uniformly bounded. For the sake of simplicity, one considers $\Lambda = \lambda I$ and $\lambda > 0$.

Here, one can easily modify the algorithm presented by Hsu and Aquino (1999) to introduce the image error directly into the control law, even if the adaptation is frozen. From (26) and (29), it follows that the ideal control law is given by

$$\upsilon_{\upsilon}^* = \lambda G^{-1}(y_r - y), \tag{30}$$

and from the image error e_{υ}, one obtains the following image error equation

$$\dot{e}_{\upsilon} = -\lambda e_{\upsilon} - G\upsilon_{\upsilon} + \lambda(y_r - y), \tag{31}$$

or, in a more compact form,

$$\dot{e}_{\upsilon} = -\lambda e_{\upsilon} + G\tilde{\upsilon}, \tag{32}$$

with $\tilde{\upsilon} = \upsilon_{\upsilon}^* - \upsilon_{\upsilon}$. From the expression of υ_{υ}^*, one verifies that the usual parameterization for the adaptive law would be

$$\upsilon_{\upsilon} = P_{\upsilon}(y_r - y), \tag{33}$$

where $P_{\upsilon} \in \mathbb{R}^{2\times 2}$ is parameterized with the adaptive parameters. However, as shown by Hsu and Aquino (1999), this leads to crucial limitations about the prior assumptions on G, not applicable to the present problem (even when K is a constant matrix). One possible solution is to use the SDU factorization method proposed by Costa et al. (2003), where $G = S_{\upsilon}D_{\upsilon}U_{\upsilon}$ and S_{υ}, D_{υ}, U_{υ} are symmetric, diagonal and upper triangular matrices, respectively. From this method, the control signal $\upsilon_{\upsilon} = [\upsilon_{\upsilon_1} \quad \upsilon_{\upsilon_2}]^{\mathrm{T}}$ can be parameterized as

$$\upsilon_{\upsilon_1} = \Theta_1^{\mathrm{T}}\omega_1, \quad \upsilon_{\upsilon_2} = \Theta_2^{\mathrm{T}}\omega_2, \tag{34}$$

where $\Theta_1 \in \mathbb{R}^9$ and $\Theta_2 \in \mathbb{R}^6$ are the vectors of adaptive parameters, $\omega_1 \in \mathbb{R}^9$ and $\omega_2 \in \mathbb{R}^6$ are the regressor vectors given, respectively, by

$$\omega_1 = [\rho_1 \quad \rho_2 \quad \rho_1 y_1 \quad \rho_1 y_2 \quad \rho_2 y_1 \quad \rho_2 y_2 \quad \upsilon_{\upsilon_2} \quad \upsilon_{\upsilon_2} y_1 \quad \upsilon_{\upsilon_2} y_2]^{\mathrm{T}},$$

$$\omega_2 = [\rho_1 \quad \rho_2 \quad \rho_1 y_1 \quad \rho_1 y_2 \quad \rho_2 y_1 \quad \rho_2 y_2]^{\mathrm{T}},$$

with $\rho_i = y_{r_i} - y_i$. Then, defining $\tilde{v} = [\tilde{\Theta}_1^{\mathrm{T}} w_1 \quad \tilde{\Theta}_2^{\mathrm{T}} w_2]^{\mathrm{T}}$ one has that

$$\dot{e}_v = -\lambda e_v + S_v \tilde{v}, \tag{35}$$

where $\tilde{\Theta}_i = \Theta_i - \Theta_i^*$ for $i = 1, 2$. From the analysis of the image error equation, the adaptation law for $\tilde{\Theta}_1$ and $\tilde{\Theta}_2$ is given by

$$\dot{\tilde{\Theta}}_1 = \dot{\Theta}_1 = -\gamma_1 e_{v_1} w_1, \quad \dot{\tilde{\Theta}}_2 = \dot{\Theta}_2 = -\gamma_2 e_{v_2} w_2, \tag{36}$$

where $\gamma_1 \in \mathbb{R}^{9\times 9}$ and $\gamma_2 \in \mathbb{R}^{6\times 6}$, with $\gamma_i = \gamma_i^{\mathrm{T}} > 0$ for $i = 1, 2$.

Now, the following theorem can be stated.

Theorem 2. *Consider the adaptive visual servoing system described by (26) and (29), with the visual servoing controller (34) and the adaptation law (36). Assume that the reference signal $y_r(t)$ is piecewise continuous and uniformly bounded in norm, S_v is state dependent and, thus, $W \triangleq S_v^{-1}$ satisfies $\frac{1}{2}\dot{W} - \lambda W < \lambda_0 I$ for some positive λ_0 and the condition (25) is satisfied. If the camera orientation angle $\phi \in (-\pi/2, \pi/2)$, $g_{11} > 0$ and $\det(G) > 0$, the following properties hold: (i) all signals of the closed-loop system are uniformly bounded; (ii) $e_v \in \mathcal{L}_2 \cap \mathcal{L}_\infty$ and $\lim_{t\to\infty} e_v(t) = 0$.*

Proof. See Appendix A.3. □

5.4. Robustness to Kinematic Uncertainties

Considering the algorithm presented by Hsu and Aquino (1999), the end-effector position $\bar{x}$ in the cartesian space could be calculated through forward kinematics map, since the manipulator joint angles are *measurable* and the robot kinematics is *known*. Then, the relationship $\bar{x} = K^{-1} y$ could be used and v_v^* would be expressed in terms of $\bar{x}$ instead of y, that is,

$$v_v^* = \lambda K^{-1} y_r - \lambda \bar{x},$$

which leads to a flaw in the definition of controller under the condition of uncertain robot kinematics.

Indeed, even under perfect knowledge of K (calibrated camera) and without adaptation, the error in kinematics can lead to imperfect visual servoing, even for simple regulation tasks ($y_d \equiv 0$). In this case, the image error dynamics can be expressed as

$$\dot{e}_v = K J(\theta)(\hat{J}(\theta)K)^{-1}[-\lambda(e_v - K\Delta k)],$$

where $\hat{J}$ denotes a nominal Jacobian and Δk is the progressive kinematics uncertainty, that is, $r = k(\theta) + \Delta k$. Expressing $K J(\theta)(\hat{J}(\theta)K)^{-1} = I + \Delta\mathcal{B}$, one has that

$$\dot{e}_v = -\lambda(I + \Delta\mathcal{B})e_v + \lambda K(I + \Delta\mathcal{B})\Delta k,$$

where the term Δk is not vanishing and its effect is not attenuated by λ. The main reason is that, in contrast with the present algorithm (Leite et al. 2006), no direct image error feedback was used. On the other hand, using the proposed visual servoing scheme, the image error dynamics is governed by

$$\dot{e}_v = -\lambda K J(\theta)(\hat{J}(\theta)K)^{-1} e_v = -\lambda(I + \Delta\mathcal{B})e_v,$$

and for small $\Delta\mathcal{B}$, the image error e_v tends exponentially to zero as $t \to \infty$.

5.5. Simulation Results

In order to illustrate the improved robustness properties of the proposed adaptive controller, one presents simulation results obtained with a two-link robot, similar to robot manipulator used in the experimental tests. The link lengths are $l_1 = 279.4$ mm and $l_2 = 228.6$ mm, for link 1 and 2, respectively. The camera parameters are $\phi = \pi/4$ rad, $f_0 = 6$ mm, $\alpha_1 = 120$ pixels mm^{-1} and $\alpha_2 = 100$ pixels mm^{-1}. The virtual surface parameters are $z_0 = 1 \times 10^3$ mm, $\epsilon = 1 \times 10^{-1}$, $a = 5$ and $b = 1$. The controller parameters are $\lambda = 1$ s^{-1}, $\gamma_1 = 8 \times 10^{-3} I$ and $\gamma_2 = 1 \times 10^{-7} I$.

The simulations are performed in the presence of measurement noise in the vision sensor. Considering an uncertainty of 10% in l_1 and 5% in l_2 and assuming that ϕ, f_0, α_1 and α_2 are unknown, the adaptive scheme of Theorem 2 leads to Figure 5(a), which depicts the time history of the image error. Note that, the asymptotic convergence to a small residual set of 1 pixel is graphically clear. On the other hand, Figure 5(b) shows the degraded performance obtained with the non-adaptive scheme (with constant parameters) in similar condition of kinematics uncertainty.

6. Hybrid Vision–Force Control

In this section, we consider the hybrid vision–force control problem for a kinematic robot manipulator interacting with an unstructured environment. In this approach, the control goal for a given task is to perform the visual tracking of an image feature fixed on the end-effector tip, while it exerts an orthogonal contact force on an unknown smooth surface.

A cartesian control law v_c can be transformed into joint control signals by using (5), where the hybrid control law v_x is given by (7) with

$$v_{hp} = \hat{R}_{es}(I - S)\hat{R}_{es}^{\mathrm{T}} R_{be}^{\mathrm{T}} \begin{bmatrix} v_v \\ 0 \end{bmatrix}, \tag{37}$$

$$v_{hf} = \hat{R}_{es} S \hat{R}_{es}^{\mathrm{T}} v_f. \tag{38}$$

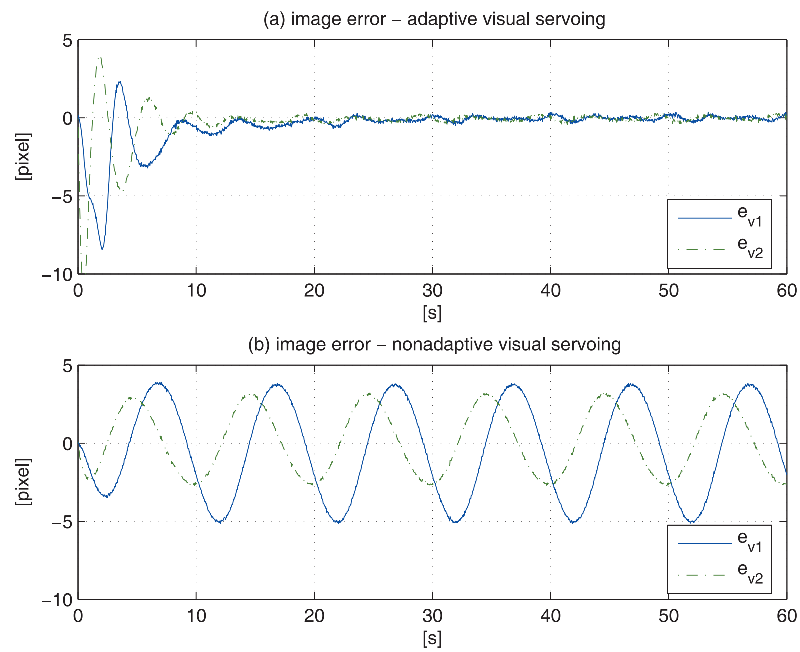

Fig. 5. Image error: (a) adaptive visual servoing; (b) non-adaptive visual servoing with fixed parameters.

Now, let $\xi_f \in \mathbb{R}^3$ be the error state vector of the decoupled closed-loop force control system $\dot{\xi}_f = A\xi_f$, where $A \in \mathbb{R}^{3\times 3}$ is Hurwitz and ξ_f is expressed in the constraint frame $\bar{E}_s$ after selecting the force control direction. Then, one can state the following theorem.

Theorem 3. *Consider the closed-loop system described by (4) and (5), with the hybrid control law given by (7) and (37)–(38), and the visual servoing controller (34) with the adaptation law (36), the force controller (15) and the orientation controller (17). Assume that: the reference signals $y_r(t)$ are piecewise continuous and uniformly bounded in norm, f_d is constant and q_d is the unit quaternion representation for $R_d \in SO(3)$; S_v is state dependent and thus $W \triangleq S_v^{-1}$ satisfies $\frac{1}{2}\dot{W} - \lambda W < \lambda_0 I$ for some positive λ_0; the condition (25) is satisfied. Under the assumptions (A1) and (A2), the following properties hold: (i) all signals of the closed-loop system are uniformly bounded; (ii) $\lim_{t\to\infty} e_v(t) = 0$, $\lim_{t\to\infty} \xi_f(t) = 0$ and $\lim_{t\to\infty} e_{qv}(t) = 0$, $\lim_{t\to\infty} e_{qs}(t) = \pm 1$. Thus, the closed-loop system is* almost *globally asymptotically stable.*

Proof. The closed-loop stability analysis uses the Lyapunov function candidate given by

$$2V = e_v^{\mathrm{T}} S_v^{-1} e_v + \tilde{\Theta}_1^{\mathrm{T}} \gamma_1^{-1} \tilde{\Theta}_1 + \tilde{\Theta}_2^{\mathrm{T}} \gamma_2^{-1} \tilde{\Theta}_2 + \xi_f^{\mathrm{T}} P \xi_f + (e_{qs} - 1)^2 + e_{qv}^{\mathrm{T}} e_{qv}.$$

The stability of the decoupled closed-loop force control system $\dot{\xi}_f = A\xi_f$ guarantees that, for a given positive-definite matrix Q there exists a positive-definite matrix P which satisfies the Lyapunov equation $A^{\mathrm{T}}P + PA = -Q$ (Khalil 2002). Since S_v is state dependent, the time derivative of V along the system trajectories is negative semidefinite, that is,

$$\dot{V} = -\lambda_0 e_v^{\mathrm{T}} e_v - \xi_f^{\mathrm{T}} Q \xi_f - e_{qv}^{\mathrm{T}} K_o e_{qv} \leq 0.$$

This implies that $V(t) \leq V(0)$ and, therefore, that e_v, ξ_f, e_{qs} and e_{qv} are uniformly bounded. The time derivative of $\dot{V}$ is given by $\ddot{V} = -2(\lambda_0 e_v^{\mathrm{T}} \dot{e}_v + \xi_f^{\mathrm{T}} Q \dot{\xi}_f + e_{qv}^{\mathrm{T}} K_o \dot{e}_{qv})$ and one can show that $\dot{e}_v$, $\dot{\xi}_f$ and $\dot{e}_{qv}$ are also uniformly bounded. Thus, $\ddot{V}$ is bounded and, hence, $\dot{V}$ is uniformly continuous.

Since V is radially unbounded and $\dot{V} \leq 0$ over the entire state space, applying the usual argument based on *Barbalat's lemma* (Khalil 2002) one has that $\lim_{t\to\infty} \dot{V}(t) = 0$ and consequently that $e_v(t) \to 0$, $\xi_f(t) \to 0$, $e_{qv}(t) \to 0$ and $e_{qs}(t) \to \pm 1$ as $t \to \infty$, which proves the *almost* global asymptotic stability of the closed-loop system. □

7. Robot Dynamic Control

Now, considering the control problem for a robot manipulator with *non-negligible* dynamics (e.g. direct-drive manipulators), an extension of the proposed controller to include the robot dynamics is presented. The non-linear dynamic model of the robot manipulator in contact with the environment can be expressed in cartesian coordinates by (Murray et al. 1994)

$$\bar{M}(\theta)\ddot{x} + \bar{C}(\theta, \dot{\theta})\dot{x} + \bar{N}(\theta) = \Gamma + f, \qquad (39)$$

where $\bar{M}$, $\bar{C}$ and $\bar{N}$ are defined in terms of the generalized coordinates namely

$$\bar{M}(\theta) = J(\theta)^{-T} M(\theta) J(\theta)^{-1},$$
$$\bar{C}(\theta, \dot{\theta}) = J(\theta)^{-T} [C(\theta, \dot{\theta}) J(\theta)^{-1} + M(\theta) \dot{J}(\theta)^{-1}],$$
$$\bar{N}(\theta) = J(\theta)^{-T} N(\theta),$$

with $\Gamma = J(\theta)^{-T}\tau$ and $f \in \mathbb{R}^3$ being the vector of contact force exerted by the end-effector on the environment.

It is worth mentioning that, in joint space, $M(\theta)$ represents the manipulator inertia matrix, $C(\theta, \dot{\theta})\dot{\theta}$ gives the Coriolis and centrifugal force terms, $N(\theta)$ includes gravity terms and τ is the vector of actuator torques. In addition, one should note that the validity of the cartesian model is restricted to motions that do not lead to a singular Jacobian matrix.

Here, the key idea is to introduce a *cascade control strategy* (Guenther and Hsu 1993) to solve the hybrid vision–force control problem for a robot manipulator with *non-negligible* dynamics, analogous to the case that only the visual servoing problem was considered (Zachi et al. 2006; Hsu et al. 2007). To achieve this, one can assume that there exists a control law

$$\Gamma = F(x, \dot{x}, x_m, \dot{x}_m, \ddot{x}_m) - f, \tag{40}$$

which guarantees the control goal defined by

$$x \to x_m(t), \quad e = x_m - x \to 0, \tag{41}$$

where x_m denotes the desired *time-varying* trajectory, expressed in the tool frame $\bar{E}_e$. Now, one supposes that it is possible to define the desired trajectory x_m and its derivatives $\dot{x}_m$, $\ddot{x}_m$ in terms of a cartesian control signal υ_x such that one has (6) except for a vanishing term, that is,

$$\dot{x} = \upsilon_x + L(p)e, \tag{42}$$

where $L(\cdot)$ denotes a linear operator with p being the differential operator. Thus, one can conclude that the hybrid control law (7) can be applied to (42).

Moreover, one can obtain some intuition if the parameters of the robot dynamic model (39) are assumed to be *exactly* known. A standard computed torque strategy could be used to solve the trajectory tracking problem, that is,

$$\Gamma = \bar{M}(\theta)[\dot{x}_m + K_d\dot{e} + K_p e] + \bar{C}(\theta, \theta)\dot{x} + \bar{N}(\theta) - f,$$

resulting in a stable closed-loop system. Then, considering $\dot{x}_m = \upsilon_x$ and from (42), one has that

$$\dot{x} = \upsilon_x + \dot{e}, \tag{43}$$

where $\dot{e}$ satisfies the closed-loop dynamics given by $\ddot{e} + K_d\dot{e} + K_p e = 0$. Hence, by a proper choice of K_d and K_p as positive definite matrices implies that $e(t), \dot{e}(t) \to 0$ exponentially as $t \to \infty$. Since this approach only differs from the kinematic control case by a vanishing term $\dot{e}(t)$, one can demonstrate that the hybrid control signal υ_x, computed for the kinematic control case, can be applied to the case of dynamic robot control and the closed-loop stability can be proved.

Note that, in the case of parametric uncertainty in the robot dynamic model (39), adaptive or robust control strategies (Sciavicco and Siciliano 2000) can also be used for the dynamic robot control (Zachi et al. 2006). Furthermore, the proposed adaptive visual servoing scheme has passivity properties which make it possible to guarantee stability when cascaded to another adaptive control system with similar passivity properties, as presented by Hsu et al. (2007).

8. Experimental Setup

This section describes the experimental setup (Figure 6) used to demonstrate the feasibility of the proposed hybrid scheme.

8.1. Hardware

The experimental results were obtained by implementing the proposed hybrid controller on a 6-DOF Zebra Zero robot manipulator (Integrated Motions, Inc.). The dynamic effects are negligible in this robot due to its large gear ratios and a high gain velocity control loop. However, due to noise sensitivity, the proportional gain in the velocity loop is not high enough to eliminate the steady state error caused by gravity effects. The gravity force acting in joints 2 and 3 (shoulder and elbow) was identified off-line using a least-squares method and effectively compensated for by adding this term to the joint control signal u in (5) (Spong and Vidyasagar 1989).

The tool consists of a rigid cylinder coupled to the robot wrist by mean of a linear spring with elastic constant given by $k_s = 64 \times 10^{-3}$ kgf mm^{-1}, aligned with the cylinder axis. This avoids hard impacts that could damage the force/torque sensor (JR3, Inc.) or the constraint surface during the interaction task. A KP-D50 CCD camera (Hitachi, Ltd.) with a lens of focal length $f_0 = 6$ mm and scaling factors $\alpha_1 = 119.0476$ pixels mm^{-1}, $\alpha_2 = 102.0408$ pixels mm^{-1} was mounted around the Zebra Zero with orientation angle $\phi \approx 0$ rad (see Figure 6). The average depth between the image frame and the robot workspace was $z_0 = 1 \times 10^3$ mm. The extracted image feature is the centroid coordinates of a red disk (or target) fixed on the end-effector tip. The images of 640×480 pixels are acquired using a Meteor frame-grabber (Matrox, Ltd.) at 30 frames per second (FPS).

8.2. Software

The visual servo controller is coded in C language and executed in 35 ms on a 200 MHz Pentium Pro processor with

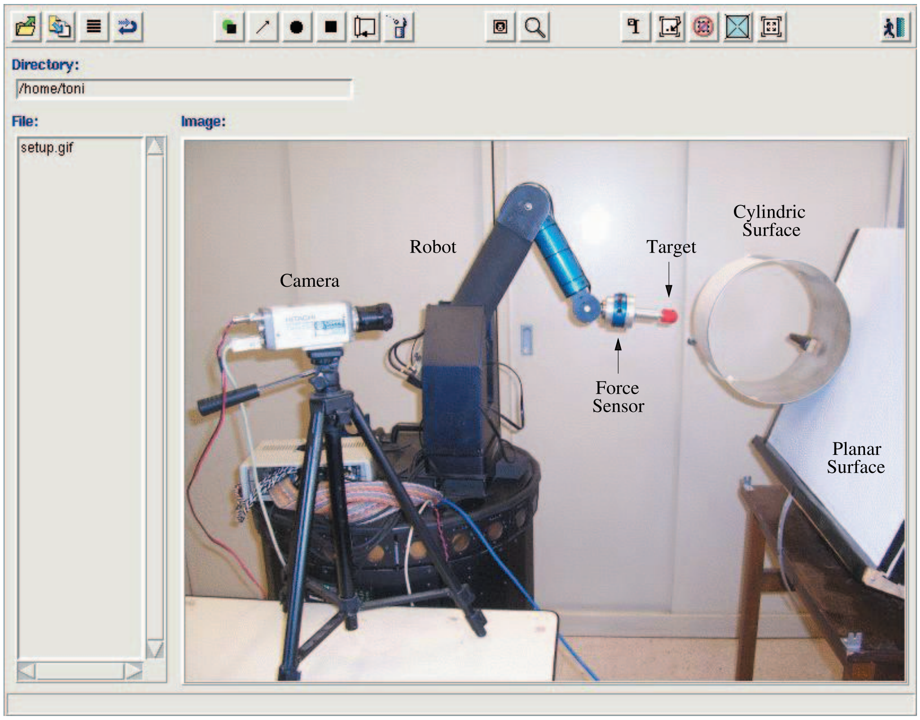

Fig. 6. Experimental station.

64 MB RAM using Linux OS. The joint velocity command generated by the hybrid control law feeds the Zebra Zero ISA board, which closes a velocity loop using an HCTL1100 microcontroller (HP Inc.) working in proportional velocity mode with 0.52 ms sampling time.

The image processing in RGB format is performed on a subwindow of 100×100 pixels wide. The first estimation of the centroid coordinates is performed off-line using an *ad-hoc* graphical user interface developed in Tcl/Tk language (Leite and Lizarralde 2006), named VServo (Figure 6). During the task execution, the image feature is computed using the image moments algorithm (Haralick and Shapiro 1993). In general, this measurement is contaminated by noise and boundary pixels can vary in an unknown pattern even in a well-conditioned environment.

9. Experiments and Results

All experimental tests were performed considering the end-effector in contact with the constraint surface and without regarding any calibration procedure. The visual servoing loop was designed to perform the tracking of a reference trajectory specified in the image frame, while the force control loop regulates the contact force to 0.6 kgf along the end-effector *approach*-axis.

The constraint surfaces were the outer side of a wooden plane and a cylindrical aluminum pipe, both fixed on the laboratory table (see Figure 6). Thus, the experiment also serves to evaluate the continuous reorientation of the end-effector during the task execution. The desired trajectory y_d is generated by the model

$$\dot{y}_d = -y_d + y_r, \tag{44}$$

with references signals

$$y_{r_1} = y_{1,0} + c_1 R_r [1 - \cos(\omega_r t)], \tag{45}$$

$$y_{r_2} = y_{2,0} + c_2 R_r [\sin(\omega_r t)], \tag{46}$$

where $y_{1,0}$ and $y_{2,0}$ are the initial position of the centroid coordinates expressed in the image frame, c_1 and c_2 are constant parameters which determine the movement direction, R_r and ω_r are the radius and the angular velocity of the reference trajectory, respectively. In the experimental tests, the robot manipulator has to perform the tracking of a circle with 40-pixel radius on the planar surface and a straight-line with 120-pixel length on the cylindric surface, both with $\omega_r = \pi/5$ rad s^{-1}.

All test cases were designed to avoid Jacobian singularities. The control parameters used in the experiments were $k_p = 40$ mm s^{-1} kgf^{-1}, $k_i = 0.4$ mm s^{-2} kgf^{-1}, $K_o = 5I$ rad s^{-1}, $\lambda = 1$ s^{-1}, $\gamma_1 = 2 \times 10^{-3} I$ and $\gamma_2 = 2 \times 10^{-4} I$. The initial conditions for the adaptive parameters $\Theta_{11}(0) = 0.2$ mm s^{-1} pixel^{-1}, $\Theta_{12}(0) = 1$ mm s^{-1} pixel^{-1}, $\Theta_{21}(0) =$

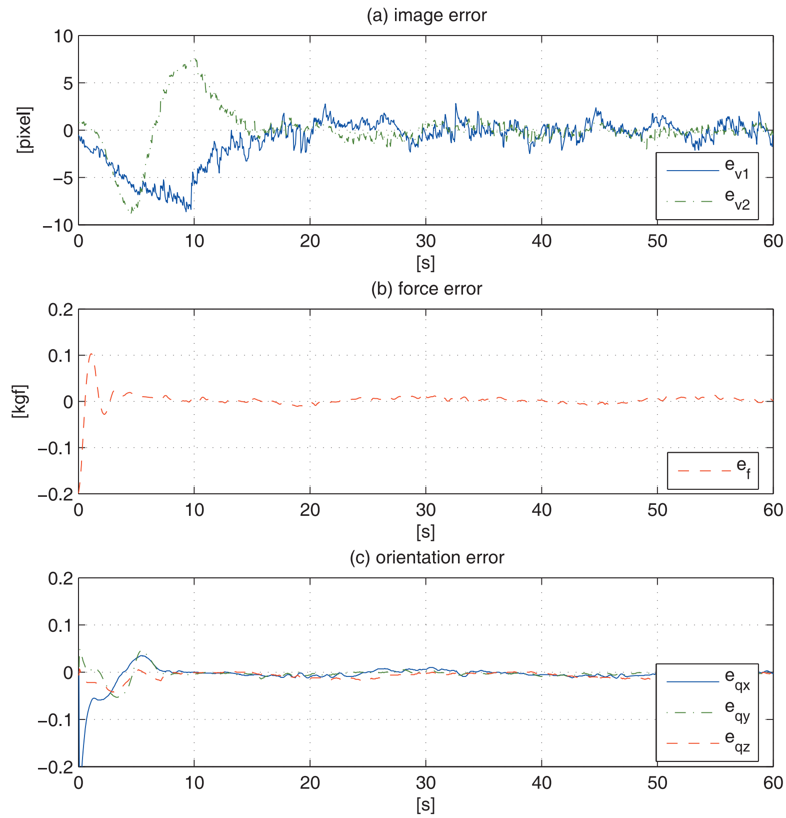

Fig. 7. Planar surface: (a) image error; (b) force error; and (c) orientation error.

-0.2 mm s^{-1} pixel^{-1}, $\Theta_{22}(0) = 1$ mm s^{-1} pixel^{-1} and $\Theta_{17}(0) = 0.1$ mm s^{-1} pixel^{-1} were obtained from the best tuning for the non-adaptive case with $\phi \approx \pi/6$ rad.

Figure 7 describes the time history of the image error, force error and orientation error, respectively, when the robot arm interacts with an *unknown* planar surface. The asymptotic convergence of the image error to a small residual set of 2 pixels is depicted in Figure 7(a). The behavior of the steady-state force error and the smooth reorientation of the end-effector on the planar surface can be observed in Figure 7(b) and (c), respectively. The maximum force error in the steady-state was 0.01 kgf and the norm of orientation error was around 5×10^{-4}. Figure 8 shows the end-effector trajectory performed on the planar surface, expressed in the image space and the cartesian space. In spite of the initial transient, a remarkable performance was achieved during the trajectory tracking, as shown in Figure 8(a).

Figure 9 describes the time history of the image error, force error and orientation error when the robot arm interacts with an *unknown* cylindric surface. It can be observed that the image error tends to a small residual region of the order of 2 pixels, as depicted in Figure 9(a). The behavior of the steady-state force error and the continuous reorientation of the end-effector on the cylindric surface can be observed in Figure 9(b) and (c), respectively. The maximum force error in the steady state was 0.02 kgf and the norm of orientation error was around 3×10^{-3}. Figure 10 shows the end-effector trajectory performed on the cylindric surface, expressed in the image space and the cartesian space. After the smooth transient, a quite good performance was achieved during the trajectory tracking, as depicted in Figure 10(a).

The estimated normal vector in some points of the trajectory performed on the constraint surface is depicted in Figure 8(b) and (c), respectively. Evaluating the end-effector trajectory in the XZ plane of the base frame, it is possible to observe the presence of small oscillations around 2 mm depth due to the arm flexibility and backlash in the robot joints gears.

10. Conclusion

In this work we have proposed a hybrid vision–force control method for the visual tracking of a desired trajectory, while keeping the robot end-effector in orthogonal contact with a smooth surface and exerting a prescribed contact force. The camera parameters, as well as the constraint surface, are assumed to be uncertain. Adaptive visual servoing is proposed to cope with the camera uncertainties and the estimation method

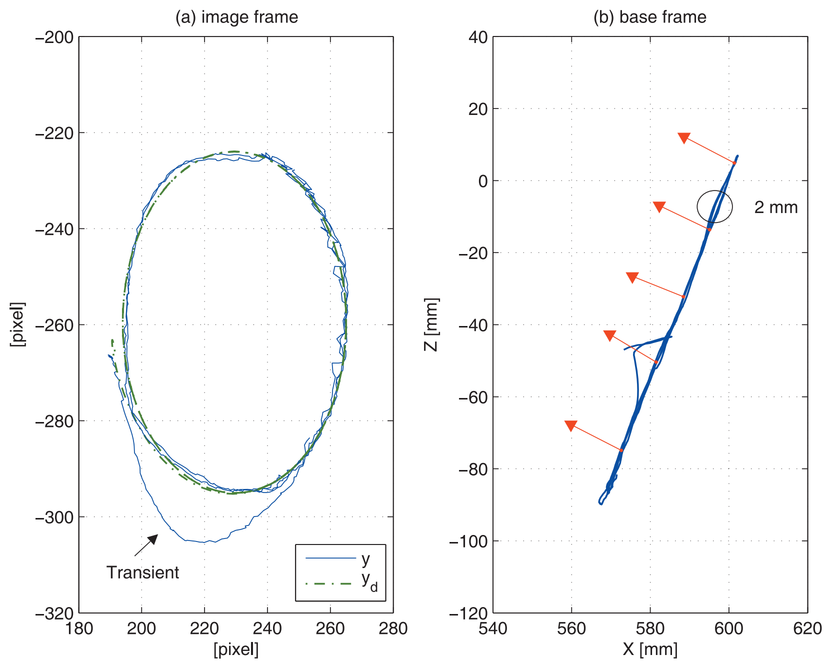

Fig. 8. Planar surface: (a) end-effector trajectory in the image frame; (b) end-effector trajectory in the XZ plane of the base frame.

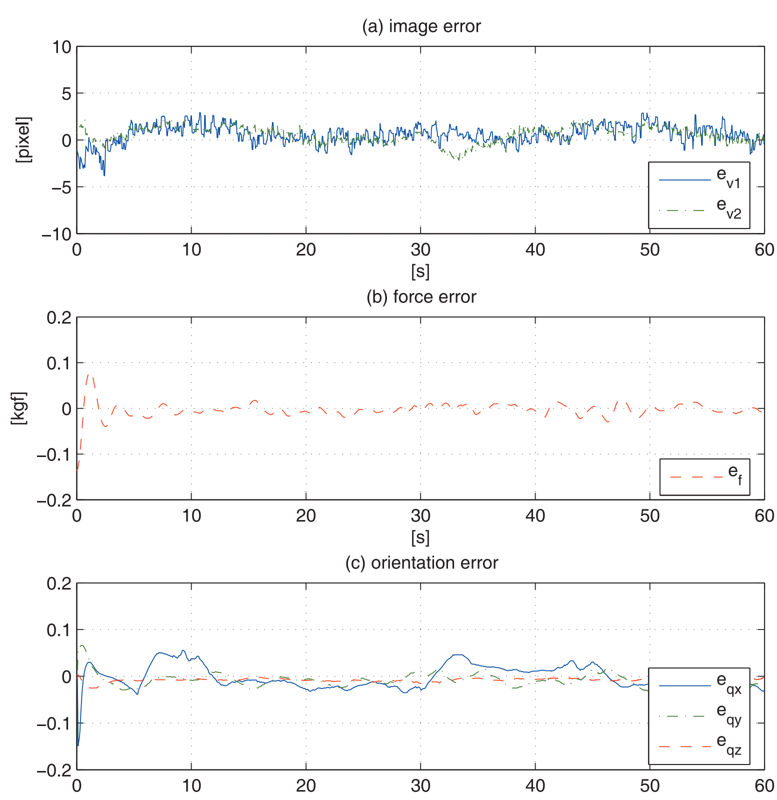

Fig. 9. Cylindric surface: (a) image error; (b) force error; and (c) orientation error.

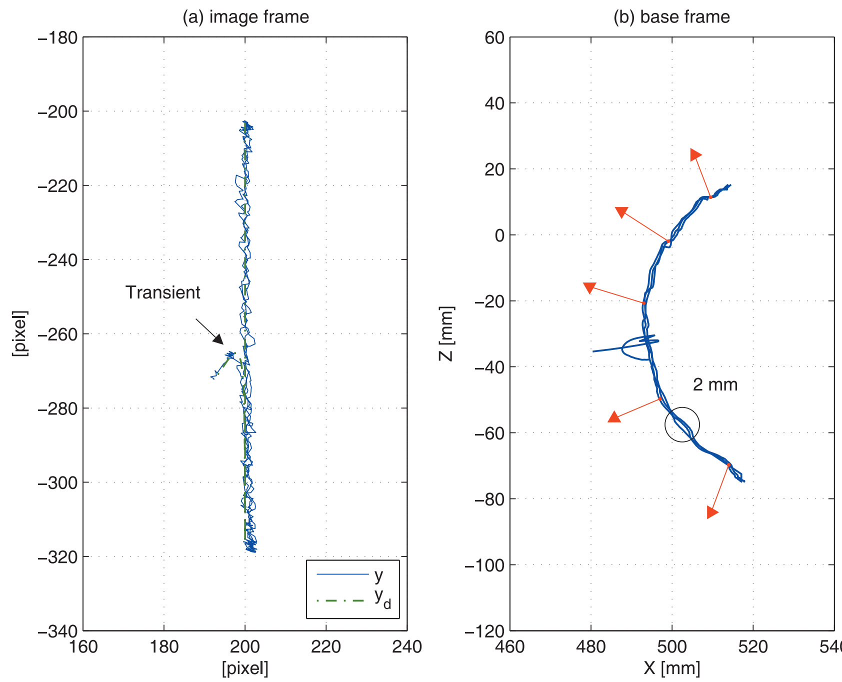

Fig. 10. Cylindric surface: (a) end-effector trajectory in the image frame; (b) end-effector trajectory in the XZ plane of the base frame.

for the constraint geometry is devised based on direct force measurements, taking into account the friction force. The stability analysis of the overall closed-loop control system has been presented. An extension of the proposed hybrid scheme to include the robot dynamics is presented based on a cascade control strategy. Experimental results show the applicability of the proposed control scheme.

A future research topic following the ideas developed here is to relax the complete knowledge of the robot kinematics and to consider the effects of the non-linearity and uncertainty in the robot dynamics.

Acknowledgment

This work was partially supported by the Brazilian agencies CAPES, CNPq and FAPERJ.

Appendix: Proofs

A.1. Orientation Control

The closed-loop stability analysis uses the Lyapunov function candidate given by

$$V = (e_{qs} - 1)^2 + e_{qv}^{\mathrm{T}} e_{qv}.$$

Let $\dot{e}_q = \frac{1}{2} J_q^{\mathrm{T}}(e_q)\tilde{\omega}$ be the error propagation equation (Wen and Kreutz-Delgado 1991), where $J_q(e_q) = [-e_{qv} \quad e_{qs} I + (e_{qv}\times)]$ and $\tilde{\omega} = (\omega_d - \omega)$. Then, differentiating V with respect to time along any system trajectory one has that $\dot{V} = e_{qv}^{\mathrm{T}}\tilde{\omega}$. Thus, setting $\tilde{\omega} = -K_o\, e_{qv}$ and considering K_o that a positive-definite matrix, one has $\dot{V} = -e_{qv}^{\mathrm{T}} K_o e_{qv} \leq 0$ is negative semidefinite. This implies that $V(t) \leq V(0)$ and, therefore, that e_{qs} and e_{qv} are uniformly bounded. The time-derivative of $\dot{V}$ is given by

$$\ddot{V} = -2e_{qv}^{\mathrm{T}} K_o \dot{e}_{qv} = e_{qv}^{\mathrm{T}} K_o e_{qs} K_o e_{qv}.$$

Thus, $\ddot{V}$ is bounded and hence $\dot{V}$ is uniformly continuous. Since V is radially unbounded and $\dot{V} \leq 0$ over the entire space, applying the usual argument based on *Barbalat's lemma* (Khalil 2002), one has that $\lim_{t\to\infty} \dot{V}(t) = 0$ and, consequently, that $e_{qv}(t) \to 0$ and $e_{qs}(t) \to \pm 1$ as $t \to \infty$. Thus, the equilibrium point $(e_{qs}, e_{qv}) = (\pm 1, 0)$ is *almost* globally asymptotically stable.

A.2. Proof of Theorem 1

The closed-loop stability analysis uses the Lyapunov function candidate given by

$$2V = \xi_p^{\mathrm{T}}\xi_p + \xi_f^{\mathrm{T}} P \xi_f + (e_{qs} - 1)^2 + e_{qv}^{\mathrm{T}} e_{qv}.$$

Since the decoupled closed-loop force control system $\dot{\xi}_f = A\xi_f$ is stable, for any given positive-definite matrix Q there exists a positive-definite matrix P that satisfies the Lyapunov equation $A^{\mathrm{T}}P + PA = -Q$ (Khalil 2002). Thus, the time derivative of V along the system trajectories is negative semi-definite, that is,

$$\dot{V} = -\xi_p^{\mathrm{T}}\bar{K}_x\xi_p - \xi_f^{\mathrm{T}}Q\xi_f - e_{qv}^{\mathrm{T}}K_o e_{qv} \leq 0,$$

where $\bar{K}_x = k_x I \in \mathbb{R}^{2\times 2}$ and $k_x > 0$. This implies that $V(t) \leq V(0)$ and, therefore, that ξ_p, ξ_f, e_{qs} and e_{qv} are uniformly bounded. The time derivative of $\dot{V}$ is given by $\ddot{V} = -2(\xi_p^{\mathrm{T}}\bar{K}_x\dot{\xi}_p + \xi_f^{\mathrm{T}}Q\dot{\xi}_f + e_{qv}^{\mathrm{T}}K_o\dot{e}_{qv})$ and one can show that $\dot{\xi}_p$, $\dot{\xi}_f$ and $\dot{e}_{qv}$ are also uniformly bounded. Thus, $\ddot{V}$ is bounded and, hence, $\dot{V}$ is uniformly continuous.

Since V is radially unbounded and $\dot{V} \leq 0$ over the entire state space, applying the usual argument based on *Barbalat's lemma* (Khalil 2002) one has that $\lim_{t\to\infty}\dot{V}(t) = 0$ and consequently that $\xi_p(t) \to 0$, $\xi_f(t) \to 0$, $e_{qv}(t) \to 0$ and $e_{qs}(t) \to \pm 1$ as $t \to \infty$, which proves the *almost* global stability of the closed-loop system.

A.3. Proof of Theorem 2

Following the SDU factorization method (Costa et al. 2003), one uses the fact that there exists an upper triangular matrix $T = U_v^{-1}$ such that $(GT) = (GT)^{\mathrm{T}} = S_v > 0$, provided that $g_{11} \neq 0$ and $\det(G) \neq 0$ (Zergeroglu et al. 1999). Then, one can rewrite (32) as

$$\dot{e}_v = -\lambda e_v - S_v[T^{-1}v_v - \lambda S_v^{-1}(y_r - y)]. \qquad (47)$$

If $g_{11} > 0$ and $\det(G) > 0$, then U_v (and U_v^{-1}) can be chosen with unitary diagonal elements and $D_v = I$, that is,

$$U_v = \begin{bmatrix} 1 & -t_{12} \\ 0 & 1 \end{bmatrix}, \quad U_v^{-1} = \begin{bmatrix} 1 & t_{12} \\ 0 & 1 \end{bmatrix}. \qquad (48)$$

One can write S_v in terms of G elements as

$$S_v = \begin{bmatrix} g_{11} & g_{11} + t_{12}g_{12} \\ g_{21} & g_{21} + t_{12}g_{22} \end{bmatrix}, \qquad (49)$$

and evaluating the symmetry condition $g_{21} = g_{11} + t_{12}g_{12}$, one has that

$$t_{12} = \frac{g_{21} - g_{12}}{g_{11}}, \quad S_v = \begin{bmatrix} g_{11} & g_{21} \\ g_{21} & s_{22} \end{bmatrix}, \quad s_{22} = \frac{(g_{21})^2 + \det(G)}{g_{11}}.$$

Thus, the ideal control law is given by

$$v_{v_1}^* = \lambda \det(G^{-1})(s_{22}\rho_1 - g_{21}\rho_2) + t_{12}v_{v_2}, \qquad (50)$$

$$v_{v_2}^* = -\lambda \det(G^{-1})(g_{21}\rho_1 - g_{11}\rho_2), \qquad (51)$$

where $\rho_i = y_{r_i} - y_i$ for $i = 1, 2$. Note that, it is not possible to obtain a linear parameterization for the control laws (50) and (51), since $v_{v_1}^*$ and $v_{v_2}^*$ include the inverse of G elements. However, one can use *Taylor series* approximation based on the assumption that the robot motions in the workspace satisfy the condition (25). Thus, one can neglect second- and higher-order terms in the series expansion. Hence, the control signal can be parameterized as $v_v = [\Theta_1^{\mathrm{T}}w_1 \quad \Theta_2^{\mathrm{T}}w_2]^{\mathrm{T}}$ and from (47) the image error equation yields $\dot{e}_v = -\lambda e_v + S_v\tilde{v}$.

Since S_v is state dependent, the gradient-type adaptive law $\dot{\Theta}_i = -\gamma_i e_{v_i} w_i$ $(i = 1, 2)$ makes the time derivative of the Lyapunov function candidate

$$2V = e_v^{\mathrm{T}}S_v^{-1}e_v + \tilde{\Theta}_1^{\mathrm{T}}\gamma_1^{-1}\tilde{\Theta}_1 + \tilde{\Theta}_2^{\mathrm{T}}\gamma_2^{-1}\tilde{\Theta}_2$$

negative semidefinite, that is, $\dot{V} = -\lambda_0 e_v^{\mathrm{T}}e_v \leq 0$. This implies that $V(t) \leq V(0)$ and, therefore, that $\tilde{\Theta}_i$ and e_v are uniformly bounded. From the image error $e_{v_i} = y_{d_i} - y_i$ one verifies that y_i is uniformly bounded, since y_{d_i} is assumed to be bounded. Noting that, $\tilde{\Theta}_i = \Theta_i - \Theta_i^*$ and $\rho_i = y_{r_i} - y_i$, where Θ_i^* is a vector of constant parameters and y_{r_i} is uniformly bounded, one concludes that Θ_i and ρ_i are also uniformly bounded. Consequently, the regressor vectors w_1 and w_2 are uniformly bounded and taking $\tilde{v} = [\tilde{\Theta}_1^{\mathrm{T}}w_1 \quad \tilde{\Theta}_2^{\mathrm{T}}w_2]^{\mathrm{T}}$ one concludes that $\dot{e}_v$ is uniformly bounded. Thus, $\ddot{V} = -2\lambda_0 e_v^{\mathrm{T}}\dot{e}_v$ is bounded and, hence, $\dot{V}$ is uniformly continuous.

Since V is radially unbounded and $\dot{V} \leq 0$ over the entire state space, applying the usual argument based on *Barbalat's lemma* (Khalil 2002) one concludes that $e_v \in \mathcal{L}_2 \cap \mathcal{L}_\infty$ and $e_v(t) \to 0$ as $t \to \infty$, which proves the global stability and asymptotic convergence of the image error.

References

Baeten, J. and De Schutter, J. (2002). Hybrid vision/force control at corners in planar robotic-contour following. *ASME Transactions on Mechatronics*, **7**(2): 143–150.

Carelli, R., Oliva, E., Soria, C. and Nasisi, O. (2004). Combined force and visual control of an industrial robot. *Robotica*, **22**: 163–171.

Chang, W.-C. (2004). Cartesian-based planar contour following with automatic hybrid force and visual feedback. *Proceedings IEEE/RSJ International Conference on Intelligent Robots and Systems*, vol. 3, pp. 3062–3067.

Costa, R. R., Hsu, L., Imai, A. K. and Kokotovic, P. (2003). Lyapunov-based adaptive control of MIMO systems. *Automatica*, **39**(5): 1251–1257.

De Schutter, J., De Laet, T., Rutgeerts, J., Decré, W., Smits, R., Aertbeliën, E., Claes, K. and Bruyninckx, H. (2007). Constraint-based task specification and estimation for sensor-based robot systems in the presence of geometric uncertainty. *The International Journal of Robotics Research*, **26**(5): 433–455.

Dean-León, E. C., Parra-Vega, V. and Espinosa-Romero, A. (2006). Visual servoing for constrained planar robots subject to complex friction. *IEEE/ASME Transactions on Mechatronics*, **11**(4): 389–400.

Duffy, J. (1990). The fallacy of modern hybrid control theory that is based on orthogonal complements of twist and wrench spaces. *Journal of Robotic Systems*, **7**(2): 139–144.

Guenther, R. and Hsu, L. (1993). Variable structure adaptive cascade control of rigid-link electrically-driven robot manipulator. *Proceedings IEEE Conference on Decision and Control*, pp. 2137–2142.

Haralick, R. M. and Shapiro, L. G. (1993). *Computer and Robot Vision*, vol. II. Reading, MA, Addison-Wesley.

Hosoda, K., Igarashi, K. and Asada, M. (1998). Adaptive hybrid control for visual and force servoing in unknown environment. *IEEE Robotics and Automation Magazine*, **5**(4): 39–43.

Hsu, L. and Aquino, P. (1999). Adaptive visual tracking with uncertain manipulator dynamic and uncalibrated camera. *Proceedings IEEE Conference on Decision and Control*, pp. 1248–1253.

Hsu, L., Costa, R. R. and Lizarralde, F. (2007). Lyapunov/passivity-based adaptive control of relative degree two mimo systems with an application to visual servoing. *IEEE Transactions on Automatic Control*, **52**(2): 364–371.

Hutchinson, S., Hager, G. and Corke, P. (1996). A tutorial on visual servo control. *IEEE Transactions Robotics and Automation*, **12**(5): 651–670.

Karayiannidis, Y. and Doulgeri, Z. (2006). An adaptive law for slope identification and force position regulation using motion variables. *Proceedings IEEE International Conference on Robotics and Automation*, pp. 3538–3543.

Khalil, H. K. (2002). *Nonlinear Systems*, vol. II (3rd edn). Englewood Cliffs, NJ, Prentice Hall.

Leite, A. C. and Lizarralde, F. (2006). Application of Tcl/Tk for a robotic system. *Proceedings of 13th Annual Tcl/Tk Conference*, pp. 1–3.

Leite, A. C., Lizarralde, F. and Hsu, L. (2006). Hybrid vision-force robot control for tasks on unknown smooth surfaces. *Proceedings IEEE International Conference on Robotics and Automation*, pp. 2244–2249.

Lippielo, V., Siciliano, B. and Villani, L. (2006). Robot interaction control using force and vision. *Proceedings IEEE/RSJ International Conference on Intelligent Robots and Systems*, vol. 3, pp. 1470–1475.

Mason, M. (1981). Compliance and force control for computer controlled manipulators. *IEEE Transactions on Systems, Man, and Cybernetics*, **11**(6): 418–432.

Murray, M., Li, Z. and Sastry, S. S. (1994). *A Mathematical Introduction to Robotic Manipulation* (1st edn). Boca Raton, FL, CRC Press.

Namvar, M. and Aghili, F. (2004). Adaptive force–motion control of coordinated robots interacting with geometrically unknown environments. *Proceedings IEEE International Conference on Robotics and Automation*, vol. 3, pp. 3061–3068.

Nelson, B. J., Morrow, J. D. and Khosla, P. K. (1995). Improved force control through visual servoing. *Proceedings of the American Control Conference*, pp. 380–386.

Olsson, T., Bengtsson, J., Johansson, R. and Malm, H. (2002). Force control and visual servoing using planar surface identification. *Proceedings IEEE International Conference on Robotics and Automation*, vol. 4, pp. 4211–4216.

Pichler, A. and Jägersand, M. (2000). Uncalibrated hybrid force–vision manipulation. *Proceedings IEEE/RSJ International Conference on Intelligent Robots and Systems*, vol. 3, pp. 1866–1871.

Raibert, M. H. and Craig, J. J. (1981). Hybrid position/force control of manipulators. *Journal of Dynamic Systems, Measurement and Control*, **102**: 126–133.

Sciavicco, L. and Siciliano, B. (2000). *Modelling and Control of Robot Manipulators* (2nd edn). Berlin, Springer.

Spong, M. W. and Vidyasagar, M. (1989). *Robot Dynamics and Control* (1st edn). New York, John Wiley & Sons.

Wen, J. T. and Kreutz-Delgado, K. (1991). The attitude control problem. *IEEE Transactions on Automatic Control*, **36**(10): 1148–1162.

Wilfinger, L. S., Wen, J. T. and Murphy, S. H. (1994). Integral force control with robustness enhancement. *IEEE Control System Magazine*, **14**(1): 31–40.

Xiao, D., Ghosh, B. K. D., Xi, N. and Tarn, T. J. (2000). Sensor-based hybrid position/force control of a robot manipulator in an uncalibrated environment. *IEEE Transactions on Control Systems Technology*, **8**(4): 634–645.

Yoshikawa, T. and Sudou, A. (1993). Dynamic hybrid position/force control of robot manipulators—online estimation of unknown constraint. *IEEE Transactions on Control Systems Technology*, **9**(2): 220–226.

Zachi, A. R. L., Hsu, L., Ortega, R. and Lizarralde, F. (2006). Dynamic control of uncertain manipulators through immersion and invariance adaptive visual servoing. *The International Journal of Robotics Research*, **25**(11): 1149–1159.

Zergeroglu, E., Dawson, D., de Queiroz, M. and Nagarkatti, S. (1999). Robust visual-servo control of robot manipulators in the presence of uncertainty. *Proceedings IEEE Conference on Decision and Control*, pp. 4137–4142.

Zhao, Y. and Cheah, C. C. (2004). Hybrid vision–force control for robot with uncertainties. *Proceedings IEEE International Conference on Robotics and Automation*, pp. 261–266.